Available online at www.sciencedirect.com

SciVerse ScienceDirect

Ceramics International 39 (2013) 171–181

CERAMICS INTERNATIONAL

www.elsevier.com/locate/ceramint

Effect of substitution of granulated slag by air-cooled slag on the properties of alkali activated slag

Hamdy El-Didamony[a], Ahmed A. Amer[a,*], Tarek M. El-Sokkary[b], Hamdy Abd-El-Aziz[b]

[a]*Faculty of Science, Chemistry Department, Zagazig University, Zagazig, Egypt*
[b]*National Research Center for Building and Housing, Dokki, Giza, Egypt*

Received 21 February 2012; received in revised form 5 June 2012; accepted 5 June 2012
Available online 15 June 2012

Abstract

This article assesses the mechanical and durability performance of replacement of GBFS by ACS activated by 3:3 NaOH:Na_2SiO_3 (3:3 SH:SSL) wt% (at optimum value 6 wt%) mixed with sea water (SW) and cured at 100% R.H. at room temperature. The kinetic behavior of activated GBFS-ACS mixes was measured by determination of setting time, combined water, bulk density and compressive strength up to 90 days. The rate of activation of the AAS has been studied from some selected samples by FT-IR, TGA, DTG analysis and SEM techniques. The compressive strength of dried activated GBFS-ACS pastes in comparison with saturated GBFS-ACS pastes up to 90 days was determined. The results revealed that the blended pastes of 80% GBFS+20% ACS gives the higher combined water, bulk density and compressive strength than those of 40/60 and 60/40% GBFS/ACS and lower than the 100% GBFS up to 90 days. Also, the compressive strength of dried samples at 105 °C for 24 h activated by (3:3 SH:SSL) mixed with SW and cured in 100% R.H. at room temperature up to 90 days is greater than saturated samples cured at the same conditions. On increasing the amount of ACS up to 40%, the setting time decreases then increases at 60% but still shorter than 100% GBFS. Finally, ACS can be used as partial substitution of GBFS in AAS.

Keywords: Alkali-activated slag; Air cooled slag (ACS); Granulated slag (GBFS); Sodium hydroxide

1. Introduction

Blast furnace slag (BFS) is a by-product generated during the manufacture of pig iron. The air cooled slag (ACS), is formed by allowing the molten slag to cool relatively slowly under ambient conditions. The cooled material is hard and dense, although it can have a vesicular texture with closed pores. The granulated blast furnace slag (GBFS) is formed by quenching molten slag with water. The very rapid cooling causes solidification of the slag as sand-sized particles of glass. The disordered structure of this glass gives the material moderate hydraulic cementitious properties when very fine ground and used as a replacement for Ordinary Portland cement (OPC) due to its latent hydraulic properties [1,2].

Cement containing water-cooled slag (WCS) has long been used in Egypt and in the world. However, there are many other unexploited slag by-product such as ACS and steel-making slag. The feasibility of utilizing these types of slags with cement has been ignored due to the judgment that ACS is hydraulically unreactive. Consequently, little of these materials is used, or their use is limited to low-value applications. A comparative study of the hydraulic reactivity of ACS and WCS produced from the same blast furnace and the same raw materials has been conducted. Although the reactivity of ACS is lower than WCS, it can still be exploited as a hydraulic material [3].

GBFS has been also investigated as an alternative binder, when activated by alkali (NaOH, Na_2CO_3, KOH, etc.) solutions, slag dissolves forms C–S–H similar to that in OPC-based concretes [4].

The world-wide need to reduce the energy used and the greenhouse gases emitted during cement manufacture has led to the pursuit of more eco-efficient materials, such as alkali-activated slag cement (AASC). Alkali activated cements are a new generation of alternative building materials, whose the

*Corresponding author. Tel.: +20 1277766533.
E-mail address: drahmed.amer@yahoo.com (A.A. Amer).

0272-8842/$36.00
http://dx.doi.org/10.1016/j.ceramint.2012.06.007

main difference from traditional Portland cements is the use of a relatively alkali-rich, clinker-free binder matrix such as alkali-activated slag (AAS) or geopolymer [5]. AAS can have high strength development and using the adequate activators can lead to rapid setting, good durability and high resistance to chemical attack [6–11]. AAS cements are sometimes referred to as geopolymers, another alternative binder. However, due to the presence of calcium in slag, which prefers to form C–S–H as the primary strength bearing phase, this classification is not entirely accurate [12,13].

The main hydration products found in AAS are C–S–H with a low Ca/Si ratio related mainly to the composition of slag and the nature of activators used, hydrotalcite intimately intermixed with the C–S–H in the MgO containing slag [14–18]. The C–S–H produced by alkali activated systems may incorporate a higher content of Al_2O_3 based on the initial composition of the slag [19,20]. A better understanding of the effects of alkaline activators such as NaOH and hydrous sodium metasilicate ($Na_2SiO_3 \cdot 5H_2O$) on the hydration mechanisms of alkali activated slag could indicate ways to optimize the use of alkaline activators [21].

In a previous study [22] it has been found that the increase of sodium hydroxide/sodium silicate liquid (SH/SSL) mixed activator for alkali activated slag content and mixed with sea water (SW) increase the combined water contents whereas, the bulk density and compressive strength increased with Na_2SiO_3 content up to 90 days.

The behavior and durability of AAS mortars and concretes have been extensively studied [23–27]. It has been shown that they can develop comparable, and greater, mechanical strength than OPC mortars [23,24]. These materials are also highly sulfate, sea water and acid resistant [25–27]. All these properties are essentially associated with the special nature of the main hydration product which is a less basic and more highly polymerized C–S–H gel than formed in OPC pastes with low porosity of the mortar and concrete [28–31].

The aim of the present investigation is to study the physico-mechanical properties of granulated slag replaced with air-cooled slag activated by (3:3 SH:SSL) wt% mixed with sea water (SW) then cured at 100% R.H. The kinetic of activation can be studied by determining the setting times, combined water, bulk density and compressive strength up to 90 days. The rate of activation of the AAS can be also studied from some selected samples by using FT-IR, TGA, DTG and SEM techniques.

2. Experimental techniques

2.1. Materials

The materials used in this work are Granulated Blast Furnace Slag (GBFS) and Air Cooled Slag (ACS) which were provided by Iron and Steel Company, Helwan, Egypt. ACS is produced by slow cooling in air whereas, the GBFS was sudden cooled by a jet of water to prevent crystallization. NaOH (SH) was produced by SHIDO Company with purity 99%, commercial sodium silicate liquid (SSL) consists of 32% SiO_2 and 17% Na_2O with silica moduls SiO_2/Na_2O equal 1.88 and density 1.46 g/cm^3 was used [22].

The chemical composition of the starting materials was shown in Tables 1 and 2.

The X-ray diffraction (XRD) pattern of ACS is shown in Fig. 1. It indicates that the ACS is completely crystalline and consists of Wadalite, syn(W) ($Ca_{12}Al_{10.6}Si_{3.4}O_{32}Cl_{5.4}$), Mullite, syn(Ms) ($Al_{4.64}Si_{1.36}O_{9.68}$), Serbro-dolskite, syn(S) ($Ca_2Fe_2O_5$), Opal-A(O) ($SiO_2 \cdot xH_2O$), Quartz (SiO_2) and Mullite (M) ($3Al_2O_3 \cdot 2SiO_2$).

Fig. 2 illustrates the XRD of GBFS. It is clear that the GBFS is nearly completely vitreous with an amorphous structure.

GBFS and ACS were firstly crushed in a jaw crusher to pass through 2 mm diameter sieve, then passed through a magnet to remove any contamination of iron melt, then ground in steel ball mill to reach 4500 ± 50 cm^2/g surface area. Different mixes were prepared from GBFS and ACS as shown in Table 3. In an earlier research [32] it was found

Table 1
Chemical composition of starting materials (wt%).

Oxide (%)	SiO_2	Al_2O_3	Fe_2O_3	CaO	MgO	SO_3	Na_2O	K_2O	L.O.I.
GBSF	37.81	13.14	0.23	38.70	7.11	1.19	1.03	0.19	–
ACS	35.60	12.43	4.95	38.35	6.09	1.32	1.21	0.11	–

Table 2
Chemical analysis seawater [22].

Test	pH	Cl^{-} [a]	SO_4^{2-} [a]	Ca^{2+} [a]	Na^{+} [a]	K^{+} [a]	Mg^{2+} [a]	TDS [b]
Sea water	8.13	22,300	1450	210	11,520	477	1341	43,300

[a] ppm unit.
[b] Total dissolved solids.

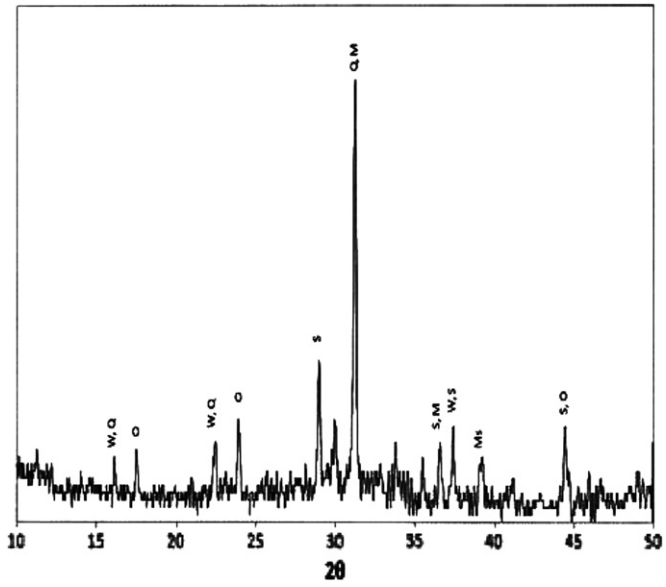

Fig. 1. XRD pattern of air cooled slag.

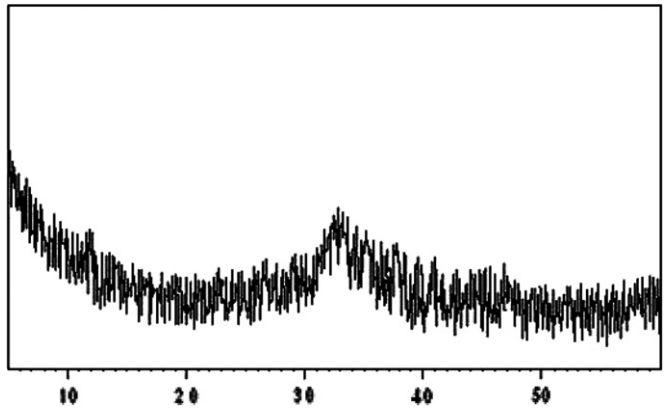

Fig. 2. XRD pattern of granulated blast furnace slag.

Table 3
Mix composition of the investigated mixes, wt%.

Mix. no.	GBFS	ACS	SH: SSL, wt%
M0	100	0	3:3
M1	80	20	3:3
M2	60	40	3:3
M3	40	60	3:3

that 6 wt% of NaOH is the optimum amount for the activation of slag. The pastes were prepared using sodium hydroxide 3% NaOH (SH) and sodium silicate liquid 3% Na_2SiO_3 (SSL) as activators at 6 wt% of dry mixes. Slag was mixed with sea water (SW) and cured in 100% relative humidity (R.H.). The water to binder ratio (w/b) was 0.26. (N.B. All water was considered, including water from water glass and hydroxide).

2.2. Preparation of pastes

The dry mix was placed on smooth, non-absorbent surface, a crater was formed in the center and the mixing water at 0.26 with the activator was poured into the crater. The water of consistency for GBFS and/or GBFS-ACS mixture was determined according to ASTM specification [33]. The mixture was slightly troweled to absorb the water for about 1 min, then completed by vigorous mixing for 3 min. The paste was strong manually molded in one inch cubic molds. The surface of the pastes was then smoothed by thin edged trowel. Immediately after molding, the specimens were cured in 100% R.H. at room temperature 23 ± 2 °C for the first 24 h, then demoulded and cured in the humidifier up to 3, 7, 28 and 90 days.

The combined water is used as an indication for the degree of hydration of the pastes. The hydration was stopped by drying the pastes at 105 °C for 24 h, then kept in air-tight bottles till testing. The combined water content was determined from the ignition of the dried paste at 800 °C for 20 min. The bulk density and compressive strength were measured according the procedures described elsewhere [34,35].

Thermal gravimetric analysis (TGA) was carried out using DTA-50 Thermal Analyzer (Schimadzu Co., Tokyo, Japan**).** About 50 mg (-53 μm) was used at heating rate 20 °C/min under nitrogen atmosphere. For IR spectroscopy, the samples were prepared using alkali halide KBr pressed disk technique [36]. The IR analysis was recorded from KBr disks using Gensis FT-IR spectrometer in the range 400–4000 cm^{-1} after 256 scans at 2 cm^{-1} resolution.

The scanning electron microscope (SEM) was taken with *Inspect S* (FEI Company, Holland) equipped with an energy dispersive X-ray analyzer (EDX). SEM was used to examine the microstructure of the fractured composites at the accelerating voltage of 200 V–30 kV and Power zoom magnification up to 300,000 ×. The samples dried at 105 °C were bonded on the sample holders with conducting glue carbon. The morphologies of the products are observed at microscopic level.

3. Results and discussion

3.1. Replacement of GBFS by ACS mixed with sea water and cured at 100% R.H.

3.1.1. Setting time

Setting time of alkali activated slag of GBFS and/or GBFS-ACS blends is graphically plotted in Fig. 3. It is clear that the setting times of GBFS replaced by 20, 40 and 60 wt% of ACS are shorter than those of 100% GBFS (M0). This may be due to that ACS acts as a nucleating agent [37]. Although the ACS has crystalline character but it contains amount of iron oxide (4.95%). This oxide dissolves from ACS containing significant levels of network forming Fe^{3+} under slightly alkaline conditions. The re-precipitation of dissolved Fe^{3+} was much faster than

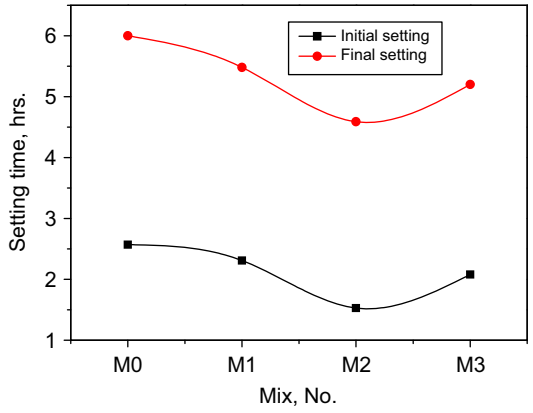

Fig. 3. Setting time of activated GBFS-ACS pastes with time.

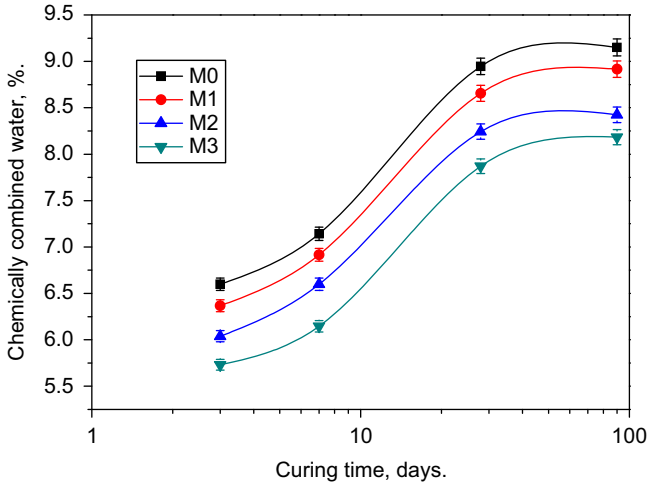

Fig. 4. Combined water of activated GBFS-ACS blends as a function of curing time.

the re-precipitation of Si^{4+} and Al^{3+} as $Fe(OH)_3$. This is likely to have a similar effect of precipitation of $Ca(OH)_2$, removing OH^- ion from the solution phase [38] and therefore shortens the setting times. On the other hand, as the amount of ACS increases the setting times diminish up to 40% ACS then elongates at 60% ACS. This is due to the fact that at 20 and 40% ACS, the amount of iron oxide has effectiveness to shorten the setting times while at 60 wt% of ACS, the reactivity of AAS decreases leading to elongate the setting time but it is still shorter than M0.

3.1.2. Chemically combined water

Chemically combined water contents of activated GBFS and/or GBFS-ACS blends as a function of curing time are graphically plotted in Fig. 4. It is clear that the combined water contents of AAS pastes gradually increase up to 90 days. This is due to the continuous hydration and accumulation of hydrated products in some of open pores that increase the combined water content. GBFS (M0) activated with 3:3 SH:SSL gives the higher value of combined water at all ages of hydration. Also, as ACS content increases the combined water decreases. This is attributed to the decrease of hydration rate of ACS [4].

3.1.3. IR spectroscopy

Fig. 5 represents the IR spectrum of anhydrous GBFS. It contains two main bands at 492 and 988 cm^{-1} as well as two less intense bands at 717 and 1422 cm^{-1}. Bands at 988 and 492 cm^{-1} imply the presence of orthosilicate unit $[Si_2O_7]^{6-}$ with partial substitution of Si^{4+} by Al^{3+} in tetrahedral positions. These units are built of two silicooxygen (or silico/and aluminooxygen) tetrahedral, connected with oxygen bridge. These two bands represent the internal vibrations for $[SiO_4]^{4-}$ and $[AlO_4]^{5-}$ tetrahedral [39]. The first comes from Si(Al)–O anti-symmetric stretching vibrations; the second should be assigned to bending vibration of O–Si–O bonds [40]. The appearance of the most intense band at relative low wave numbers proves the silicate phases in the slag containing orthosilicate units $[Si_2O_7]^{6-}$. The existence of the weak band at 717 cm^{-1}, assigned to the symmetric stretching vibration of the Si–O–Si(Al) bridges, which confirms the presence of these units. It is also possible to suppose that it is also connected with vibrations of Si–O–Al bridges formed by linkage between $[SiO_4]^{4-}$ and $[AlO_4]^{5-}$ tetrahedral [41]. Moreover, it is impossible to exclude the association of this band with Al–O vibrations, appearing in alumino-silicates octahedral. High content of aluminum shifts the band 988 cm^{-1} at such low wave number. Aluminum atoms in tetrahedral coordination shift of the most intense band to lower wave numbers, in relation to 1100 cm^{-1} position characteristic for pure silica spectra in non-hydrated form [42]. Low intensity bands at 1422 cm^{-1} originates from carbonate groups $[CO_3]^{2-}$. High full width at half maximum (FWHM) especially in the case of the most intense band at 988 cm^{-1} proves the significant content of glassy phase in the slag. It is known that the phases of non-ordered structure increase the band width due to the existence of significant fluctuations of geometric parameter. The shape of the spectra is typical of glassy aluminosilicates belonging to the groups of gehlenites and melilites [43].

The IR spectra of the AAS with 3:3 SH:SSL mixed with SW and cured up to 90 days are seen in Fig. 5. The main absorption band which is related to Si–O (Al) anti-symmetric stretching vibration in case of (GBFS) at 988 cm^{-1} is shifted to 972 and 971 cm^{-1} with a decrease in width of the bands at 3 and 90 days, respectively. This fact should be related to the increase of crystallinity of the sample caused by ordering of the structure [44]. Absorption bands at 3448–3456 cm^{-1} and at 1647–1653 cm^{-1} are related to stretching of O–H groups and bending vibration of H:OH, respectively. These bands disappear in anhydrous GBFS due to that there are no any hydration products such as C–S–H, C–A–H and C–A–S–H. Absorption bands of water are due to lattice H_2O of the hydrated C–S–H, C–A–H as well as C–A–S–H. These values confirmed the formation of the geo-polymer [45]. Absorption bands at 1422–1472 cm^{-1} are assigned to atmospheric

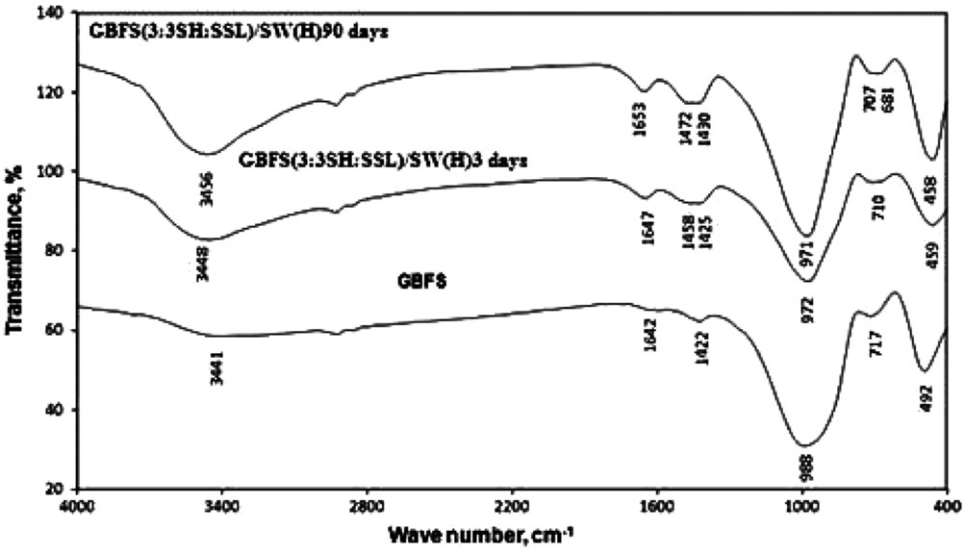

Fig. 5. FT-IR spectra of anhydrous GBFS and slag pastes activated by (3:3 SH:SSL) mixed with SW and cured up to 90 days.

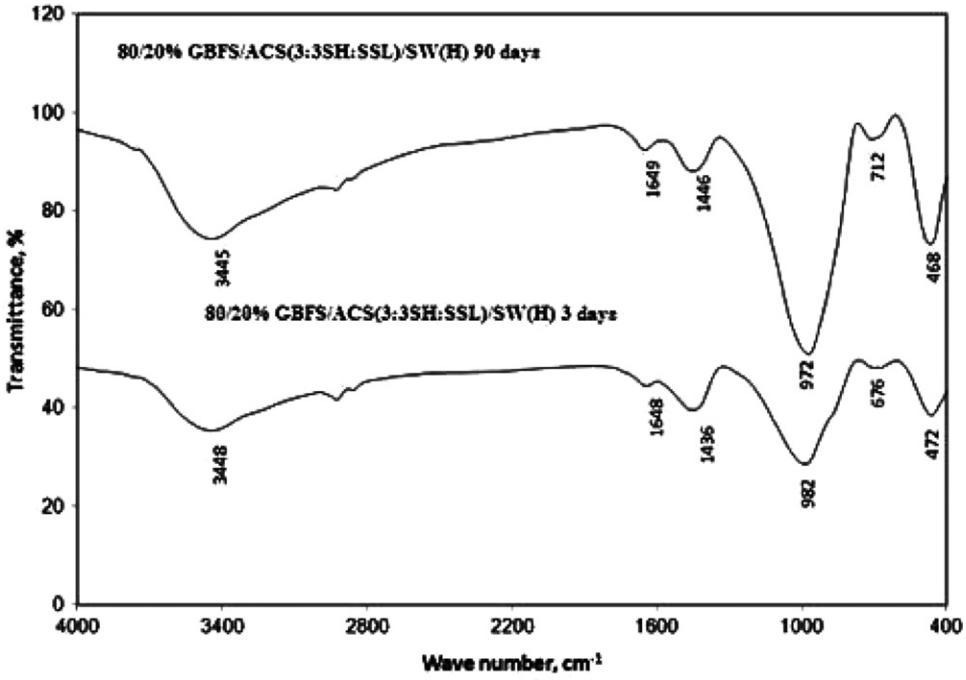

Fig. 6. FT-IR spectra of activated 80% GBFS+20% ACS pastes cured for 3 and 90 days.

carbonation. Bands at 681–717 and 458–492 cm^{-1}, sample at 90 days, which are related to symmetric stretching vibrations of the Si–O–Si (Al) bridges and O–Si–O bending vibrations have high intensity and low of (FWHM) than those of 3 day and anhydrous GBFS at 710–717 cm^{-1}. This is due to the increase of geo-polymer formation and also the glassy phase of the sample. The peak intensity of both bands at 1647–1653 cm^{-1} and 3448–3456 cm^{-1} at 90 days is bigger than those at 3 days due to the increase of the amount of C–S–H, C–A–H and C–A–S–H after activation.

Fig. 6 represents the FTIR spectra of activated 80% GBFS+20% ACS cured for 3 and 90 days. It is clear that the absorption bands at 468–472 cm^{-1} are due to O–Si–O bonds bending vibration. Absorption bands at 676–712 cm^{-1} are related to symmetric stretching vibrations of the Si–O–Si (Al) bridges. Also, strong absorption bands at 972–982 cm^{-1} is due to Si(Al)–O anti-symmetric stretching. Absorption bands at 3448–3445 cm^{-1} and at 1648–1649 cm^{-1} are related to stretching of O–H groups and bending vibration of H:OH, respectively. The bands intensity increases from 3 up to 90 days due to the continuous activation and formation of geo-polymers as well as hydrated products [45]. Absorption bands at 1436–1446 cm^{-1} are assigned to atmospheric carbonation. The bands intensity at both 1648–1649 cm^{-1} and 3445–3448 cm^{-1} at 90 day is bigger than that at 3 day due to the large amount of C–S–H, C–A–H as well as C–A–S–H.

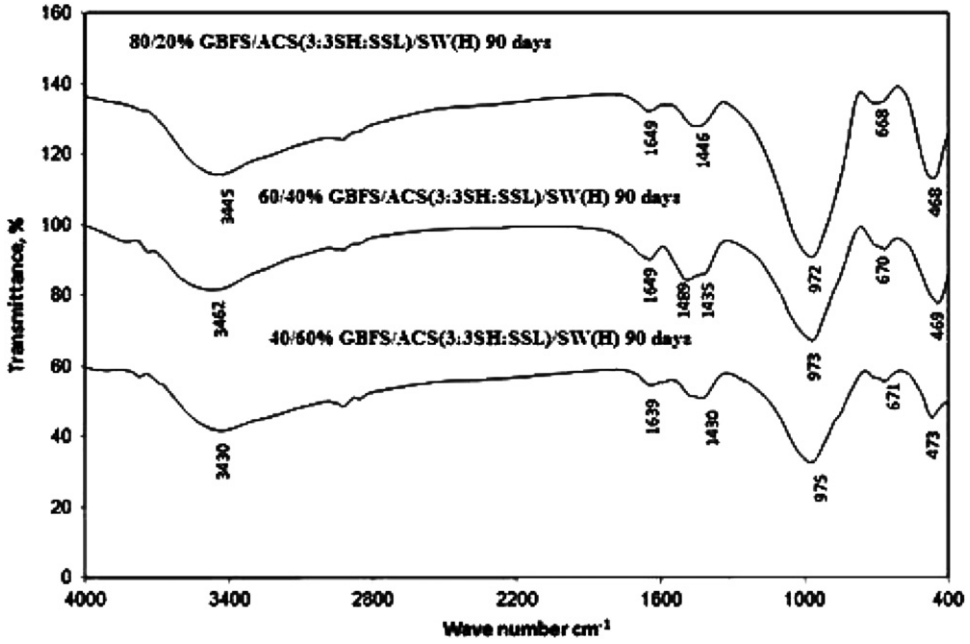

Fig. 7. FT-IR spectra of activated 80, 60 and 40% GBFS+20, 40 and 60% ACS and cured for 90 days.

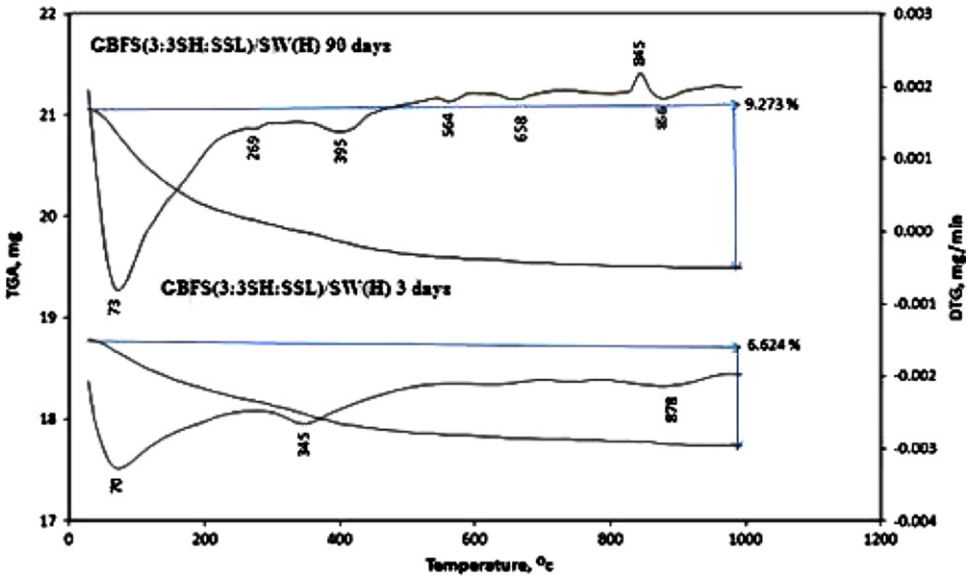

Fig. 8. TGA and DTG of activated GBFS and cured for 3 and 90 days.

Fig. 7 illustrates the FTIR spectra of 20, 40 and 60 wt% ACS instead of GBFS and cured at 100% R.H. for 90 days. The individual bands of activated slag are identical but with slight differences in intensity and (FWHM) of the bands. The bands at 468–473 cm^{-1} due to O–Si–O bending vibration, absorption bands 668–671 cm^{-1} related to symmetric stretching vibrations of the Si–O–Si (Al) bridges. The band at 972–975 cm^{-1} related to Si (Al)–O anti-symmetric stretching vibration. The bands at 1639–1649 and 3430–3462 cm^{-1} assigned to bending vibration of H:OH and stretching of O–H group, respectively. The bands of M1 are greater than M2 and M3. This is due to that ACS is more crystalline than GBFS which has low rate of hydration and formation of geo-polymers as well as hydrated products. The weak absorption bands at 1430–1446 cm^{-1} are due to atmospheric carbonation.

3.1.4. Thermo gravimetric analysis

Fig. 8 presents TGA and DTG of GBFS activated by (3:3 SH:SSL) mixed with SW and cured for 3 and 90 days. The weight loss at 1000 °C was 6.624% and 9.273% for samples activated for 3 and 90 days, respectively. This is due to the continuous hydration and formation of more hydration products up to 90 days. Endotherms at 70 and 73 °C are due to the dehydration of free water and C–S–H from hydrated cement matrix [46]. The endothermic peaks

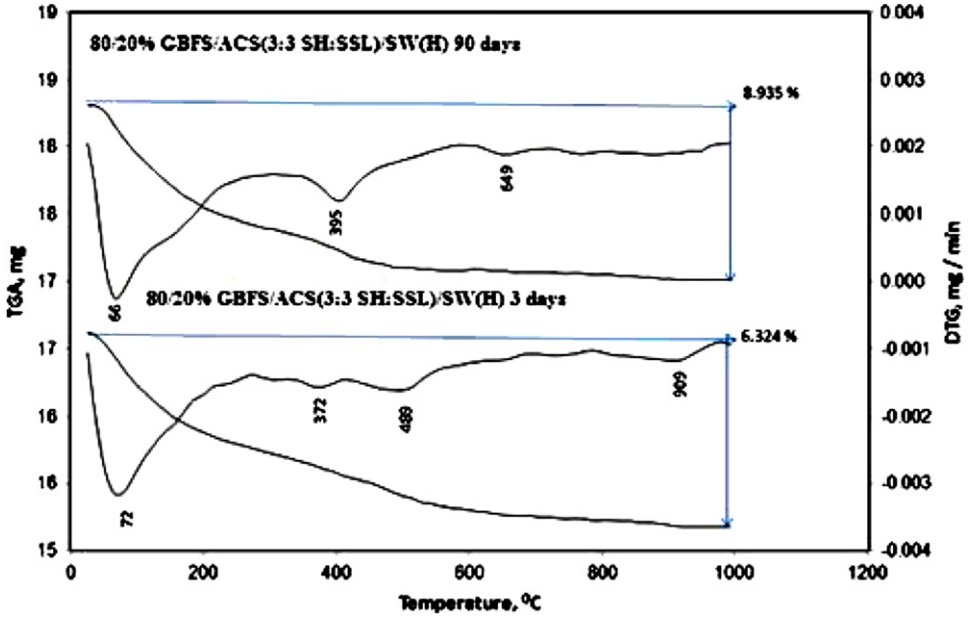

Fig. 9. TGA and DTG of activated 80% GBFS+20% ACS and cured for 3 and 90 days.

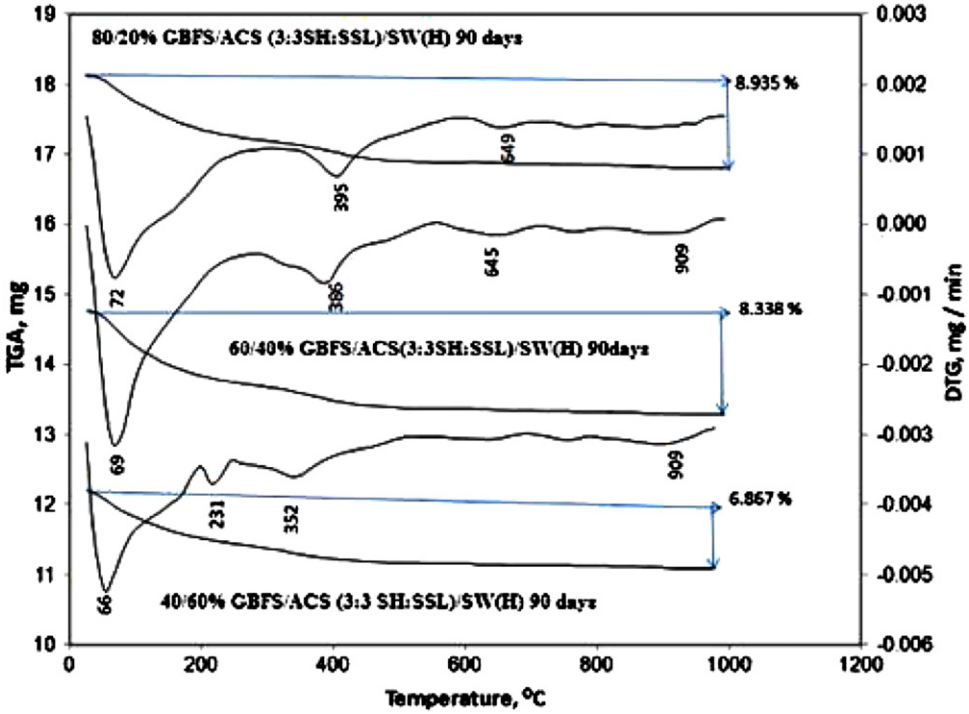

Fig. 10. TGA and DTG of activated 80, 60 and 40% GBFS+20, 40 and 60% ACS and cured for 90 days.

at 269, 345 and 395 °C related to C–A–H and C–A–S–H [47]. The endothermic peaks at 564–658 °C are related to the decomposition of carbonate, hydrated aluminates and final stage of decomposition of C–S–H [3]. Exothermic peak at 845 °C is due to crystallization of β-wallastostonite [48]. Endothermal peak at 878 °C is due to the decomposition of well crystallized $CaCO_3$.

Fig. 9 illustrates the TGA and DTG of M1 (80/20) activated by (3:3 SH:SSL) and cured for 3 and 90 days. The weight loss at 1000 °C was 6.324% and 8.935% for pastes after 3 and 90 days, respectively. The increase of weight loss at 90 day is due to the continuous hydration. DTG shows the peaks which related to this loss. Endothermic peaks at 66 °C and 72 °C are due to the dehydration of free water and interlayer water of C–S–H [46]. Endothermic peak at 372 °C related to the decomposition of hydration products (C–A–H and C–A–S–H) [47]. The endotherm located at 3 day is shifted to 395 °C at 90 day due to the increase of crystallinity of activated paste with curing time. The endothermic peak at 489 °C at 3 day is due to the

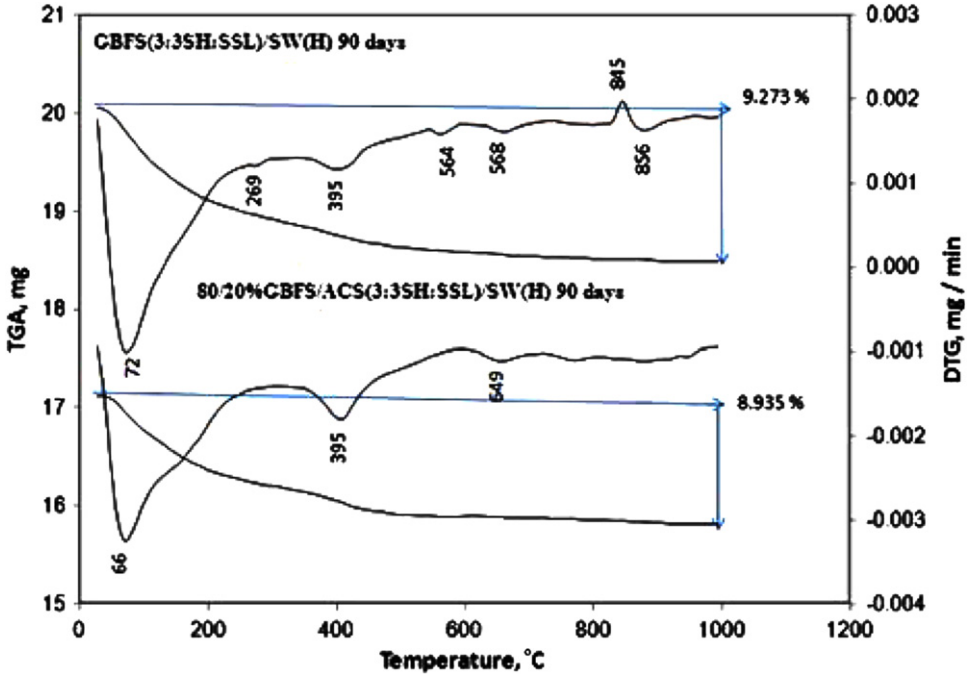

Fig. 11. TGA and DTG of activated 100% GBFS and 80% GBFS+20% ACS and cured at 90 day.

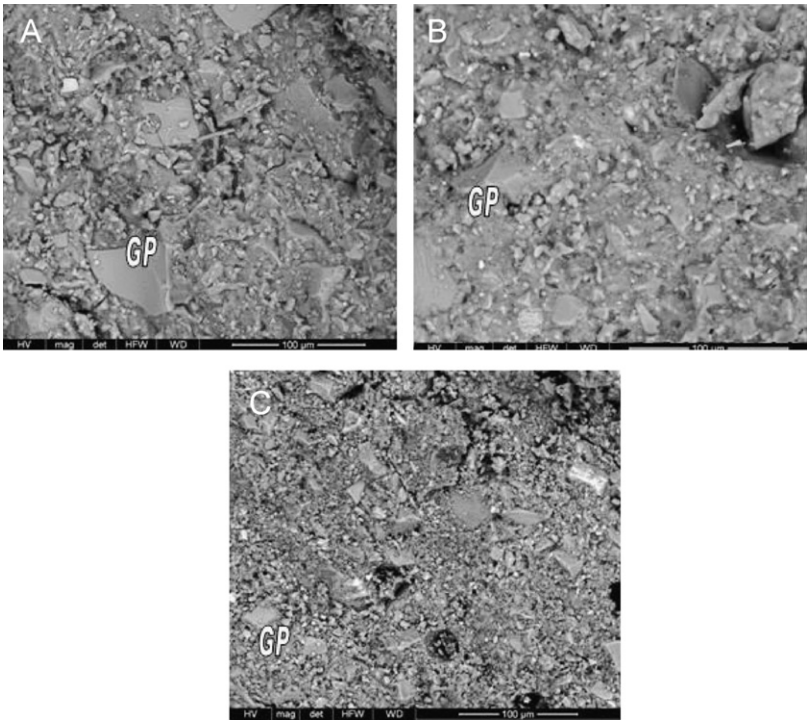

Fig. 12. SEM of (A) 100%GBFS, (B) 80/20% and (C) 40/60% GBFS/ACS pastes activated with 3:3 SH:SSL mixed with SW and cured in 100% R.H. at 12 months.

decomposition of $Ca(OH)_2$ which is completely consumed with time up to 90 days. The endotherm at 649 °C corresponds to the decomposition of carbonate, hydrated aluminates and final stage of decomposition of C–S–H [3].

Fig. 10 shows the TGA and DTG of M1, M2 and M3 activated and cured for 90 days. The weight loss of M1 (8.935%) is greater than that of M2 (8.338%) due to the higher activity of GBFS than ACS which characteristic by high crystallinity with low rate of hydration and less hydrated products. On the other hand, the DTG shows that the main temperature range of decomposition (200–400 °C) of hydration products such as (C–A–H and C–A–S–H). These endotherms are shifted to higher temperature with ACS content. This is due to the decrease of

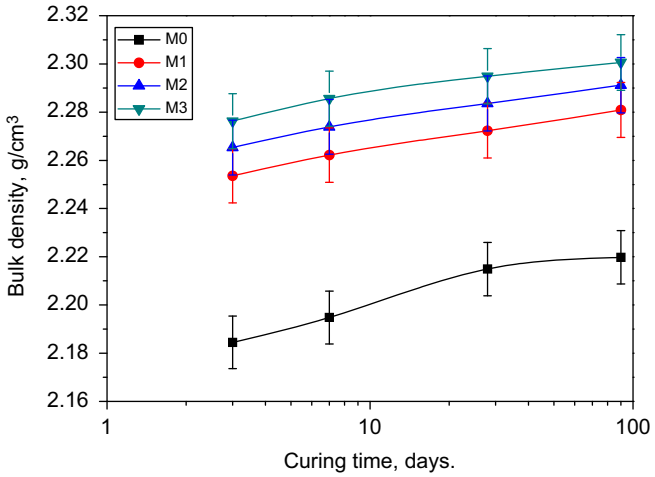

Fig. 13. Bulk density of activated GBFS-ACS and cured up to 90 days.

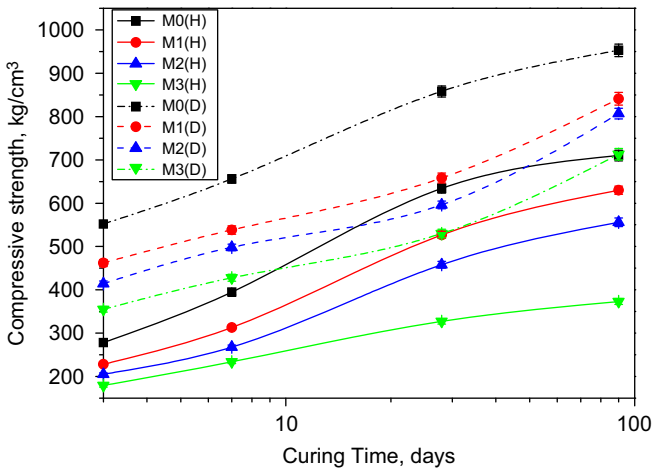

Fig. 14. Compressive strength of activated GBFS-ACS blends cured in 100% R.H. as well as dried at 105 °C up to 90 days.

the hydration products with ACS which are early decomposed at lower temperature.

Fig. 11 illustrates the TGA and DTG of M0 and M1 activated and cured for 90 days. The weight loss of M0 (9.273%) is greater than M1 (8.935%). This is due to that the hydration rate of M0 (100% GBFS) is greater than M1 (80% GBFS+20%ACS). M0 shows an exothermic peak at 845 °C which is due to the recrystallization of β-wallastostonite from the decomposition of CSH of GBFS activated slag [48].

3.1.5. Scanning electron microscopy

The SEM micrographs of hardened GBFS and/or GBFS+ACS activated slag mixed with SW and cured for 12 months are shown in Fig. 12. It is clear that from SEM observation of M0 paste Fig. 12A is more homogeneous and very compact than mixes M1 and M2 Fig. 12 B and C. This is due to the increase of dissolution of activated species (Al^{3+}, Si^{4+} and Ca^{2+}) of M0 sample which sufficient to form long chains of geopolymer of cross linkage geopolymer with compact structure. While in case of M1 and M3 the dissolution of activated species decreases. This is not enough to sustain geopolymerization forming short chain of geopolymer (poorly crystalline structure). On the other hand, as the amount of ACS increases the geopolymerization and hydration reaction decrease due to the low activity of ACS in comparison with GBFS [3].

3.1.6. Bulk density

The bulk density of hardened GBFS and/or GBFS+ACS activated slag and cured in 100% R.H. up to 90 days is plotted in Fig. 13. It clear that the bulk density increases with curing time up to 90 days for all cement pastes due to the continuous formation of hydrated products. These are deposited in the open pores that increase the bulk density of the activated slag. On the other hand, as the amount of ACS increases the bulk density of activated slag paste increases. This is due to the high specific gravity of ACS in comparison with GBFS. The specific gravity of granulated slag is 2.1 and that of ACS is 2.6 [49]. It can be said that the increase of bulk density of activated slag with ACS is mainly due to the increase of its specific gravity and not for the formation of more hydrated products.

3.1.7. Compressive strength

The compressive strength of hardened GBFS and/or GBFS+ACS activated and cured in 100% R.H. as well as dried at 105 °C up to 90 days is graphically represented in Fig. 14. The compressive strength of all mixes increases with curing time. M0 shows the higher values of compressive strength at all ages of hydration. As the amount of ACS increases, the compressive strength decreases. This is due to the low activity of ACS in comparison with GBFS [3]. From the figure it is clear that M3 has a slow rate of strength increase due to the higher content of ACS that leads to decrease the rate of hydration as well as formation of hydrated products which responsible for the compressive strength. The compressive strength of dried activated slag-air cooled slag pastes at 105 °C for 24 h is increases with curing time. Also, the compressive strength of M0 shows higher values than M1, M2 and M3 due to the higher reactivity of GBFS as well as highly dissolution of activated species (Si^{4+}, Al^{3+} and Ca^{2+}) which are share in pozzolanic and geopolymeric reaction. On the other hand, the compressive strength of dried activated slag pastes is greater than that saturated slag pastes cured at 100% R.H. This is due to that the activity of slag increases with temperature [50]. The drying acts as self autoclaving which increases the strength [51]. Compressive strength of M1, M2 and M3 sharply increases from 28 up to 90 days but still lower than M0 due to its reactivity at later ages as result of nucleation reaction which leads to filling mo. then re-open pores and therefore increases the compressive strength.

4. Conclusion

The main conclusions could be derived from this investigation are summarized as follows:

1. The setting times of alkali activated slag shorten with the amount of ACS content.
2. The blend of 80/20% (GBFS/ACS) gives higher combined water, bulk density and compressive strength than those of 60/40 and 40/60% (GBFS/ACS) and lower than 100% GBFS up to 90 days.
3. The compressive strength of dried samples at 105 °C for 24 h activated by (3:3 SH:SSL) mixed with sea water and cured in 100% R.H. at room temperature up to 90 days is greater than those cured at 100% R.H.
4. ACS can be used as partial substitution of GBFS in AAS.

Acknowledgment

The authors are grateful to thank Dr. Ahmed A. Amer, Assoc. Professor, Faculty of Science, Zagazig University for his great help throughout the interpretation of the results of this article.

References

[1] G. Hendrik, H.G. van Oss, Slag-Iron and Steel, 69, US Geological Survey Minerals Year Book, 2003, pp. 1–7.
[2] A.R. Sakulich, Reinforced geopolymer composites for enhanced material greenness and durability, Sustainable Cities and Society 1 (2011) 195–210.
[3] N.Y. Mostafa, S.A.S. El-Hemaly, E.I. Al-Wakeel, S.A. El-Korashy, P.W. Brown, Characterization and evaluation of the hydraulic activity of water-cooled slag and air-cooled slag, Cement and Concrete Research 31 (2001) 899–904.
[4] C. Li, H. Sun, L. Li, A review: the comparison between alkali-activated slag (Si+Ca) and metakaolin (Si+Al) cements, Cement and Concrete Research 40 (9) (2010) 1341–1349.
[5] S.A. Bernal, R. Mejia de Gutierrez, A.L. Pedraza, J. Provis, Effect of binder content on the performance of alkali-activated slag concretes, Cement and Concrete Research 41 (2011) 1–8.
[6] M. Ben Hafa, G. Le Saout, F. Winnefeld, B. Lothenbach, Influence of activator type on hydration kinetics, hydrate assemblage and microstructural development of alkali-activated blast-furnace slags, Cement and Concrete Research 41 (2011) 301–310.
[7] M.C.G. Juenger, F. Winnefeld, J.L. Provis, J.H. Ideker, Advances in alternative cementitious binders, Cement and Concrete Research 41 (2011) 1232–1243.
[8] P. Duxson, A. Fernández-Jiménez, J.L. Provis, G.C. Lukey, A. Palomo, J.S.J. van Deventer, Geopolymer technology: the current state of the art, Journal of Materials Sciences 42 (2007) 2917–2933.
[9] V.D. Glukhovsky, G.S. Rostovskaja,G.V. Rumyna, High Strength Slag-Alkaline Cements, In: 7th International Congress Chemistry Cement (Paris), 3 (1980) pp. 164–168.
[10] H.F.W. Taylor, Cement Chemistry, 2nd Ed., Thomas Telford Publication, London, 1998.
[11] P. Duxson, J.L. Provis, G.C. Lukey, J.S.J. van Deventer, The role of inorganic polymer technology in the development of green concrete, Cement and Concrete Research 37 (2007) 1590–1597.
[12] A.R. Sakulich, E. Anderson, C. Schauer, M.W. Barsoum, Mechanical and microstructural characterization of an alkali-activated slag/limestone fine aggregate concrete, Construction and Building Materials 23 (8) (2009) 2951–2957.
[13] A.R. Sakulich, S. Miller, M.W. Barsoum, Chemical and microstructural characterization of 20-month-old alkali-activated slag cements, Journal of the American Ceramic Society 93 (6) (2010) 1741–1748.
[14] D.M.R. Brew, F.P. Glasser, The magnesia–silica gel phase in slag cements: alkali (K, Cs) sorption potential of synthetic gels, Cement and Concrete Research 35 (2005) 77–83.
[15] A. Gruskovnjak, B. Lothenbach, L. Holzer, R. Figi, F. Winnefeld, Hydration of alkali-activated slag: comparison with ordinary Portland cement, Advances in Cement Research 18 (2006) 119–128.
[16] I.G. Richardson, The calcium silicate hydrates, Cement and Concrete Research 38 (2008) 137–158.
[17] S.D. Wang, K.L. Scrivener, Hydration products of alkali activated slag cement, Cement and Concrete Research 25 (1995) 561–571.
[18] C.K. Yip, G.C. Lukey, J.S.J. van Deventer, The coexistence of geopolymeric gel and calcium silicate hydrate at the early stage of alkaline activation, Cement and Concrete Research 35 (2005) 1688–1697.
[19] I.G. Richardson, A.R. Brough, G.W. Groves, C.M. Dobson, The characterization of hardened alkali-activated blast-furnace slag pastes and the nature of the calcium silicate hydrate (C–S–H) phase, Cement and Concrete Research 24 (1994) 813–829.
[20] S.D. Wang, K.L. Scrivener, 29Si and 27Al NMR study of alkali-activated slag, Cement and Concrete Research 33 (2003) 769–774.
[21] M. Ben Hafa, G. Le Saout, F. Winnefeld, B. Lothenbach, Influence of activator type on hydration kinetics, hydrate assemblage and microstructural development of alkali-activated blast-furnace slags, Cement and Concrete Research 41 (2011) 301–310.
[22] H. El-Didamony, A.A. Amer, H. Abd-El-Aziz, Properties and durability of alkali-activated slag pastes immersed in sea water, Ceramics International 38 (5) (2012) 3773–3780.
[23] V.D. Glukhovsky, G.S. Rostovskaja, G.V. Rumyna, High Strength Slag-Alkaline Cements, In: 7th International Congress Chemistry Cement (Paris), 3 (1980) pp. 164–168.
[24] S.A. Bernal, R. Mejia de Gutierrez, A.L. Pedraza, J. Provis, Effect of binder content on the performance of alkali-activated slag concretes, Cement and Concrete Research 41 (2011) 1–8.
[25] T. Bakharev, J.G. Sanjayan, Y.B. Cheng, Sulfate attack on alkali-activated slag concrete, Cement and Concrete Research 32 (2002) 211–216.
[26] F. Puertas, R. Mejia de Gutierrez, A. Fernandez-Jimenez, S. Delvasto, J. Maldonado, Alkaline cement mortars, chemical resistance to sulphate and seawater attack, Materiales de Construccion 52 (267) (2002) 55–71.
[27] T. Bakharev, J.G. Sanjayan, Y.B. Cheng, Resistance of alkali-activated slag concrete to acid attack, Cement and Concrete Research 33 (2003) 1607–1611.
[28] J.I. Escalante-Garcia, A.F. Fuentes, A. Gorokovsky, P.E. Fraire-Luna, G. Mendoza-Suarez, Hydration products and reactivity of blast-furnace slag activated by various alkalis, Journal of the American Ceramic Society 86 (12) (2003) 48–53.
[29] A. Fernandez-Jimenez, F. Puertas, I. Sorbrados, J. Sanz, Structure of calcium silicate hydrates formed in alkaline activated slag. Influence of the type of alkaline activator, Journal of the American Ceramic Society 86 (8) (2003) 1389–1394.
[30] F. Puertas, A. Fernandez-Jimenez, M.T. Blanco-Varela, Pore solution in alkali-activated slag cement pastes. Relation to the composition and structure of calcium silicate hydrate, Cement and Concrete Research 34 (2004) 139–148.
[31] C. Shi, Strength, pore structure and permeability of alkali-activated slag mortars, Cement and Concrete Research 26 (1996) 1789–1799.
[32] M.S. Hafeez, Preparation and Characterization of the Non Portland Cement, M.Sc. Thesis, Faculty of Science, Zagazig University, Zagazig, Egypt. 2008.
[33] ASTM Designation: C-191, Standard Method for Normal Consistency and Setting of Hydraulic Cement, ASTM Annual Book of ASTM Standards, 04.01 (2008).

[34] H.H. Assal, Some Studies on the Possibility of Utilization of Calcareous Shale/Clay Deposits in Building Bricks Industry, Ph.D. Thesis, Faculty of Science, Zagazig University, Zagazig, Egypt, 1995.
[35] A.S.T.M. C109M, Standard Test Method for Compressive Strength of Hydraulic Cement Mortars, 2007.
[36] R.J. Errington, Advanced Practical Inorganic and Metal Organic Chemistry, Balckie Academic Professional, An Impient Chapman & Hall, 1997.
[37] V.K. Vlosov, The mechanism of increase of concrete strength at introduction of micro fillers, Concrete Research (USSR) 10 (1988) 9–11.
[38] V. Daux, C. Guy, T. Advocat, J.L.P. Crovisier, Stille, kinetic aspects of basaltic glass dissolution at 90 °C: role of aqueous silicon and aluminium, Chemical Geology 142 (1997) 109–126.
[39] M. Criado, A. Fernandez-Jimenez, A. Palomo, Alkali-activation of fly ash: effect of the SiO_2/Na_2O ratio. Part I: FTIR study, Micoporous and Mesoporous Materials 106 (2007) 180–191.
[40] M. Handke, Applied Spectroscopy Society for Applied Spectroscopy 40 (1986) 871.
[41] K. Ishida, D.M. Jenkins, F.C. Hawthorne, American Mineralogist 93 (2008) 1112.
[42] J. Zhang, J.L. Provis, D. Feng, J.S.J. van Deventer, Geopolymers for immobilization of Cr^{6+}, Cd^{2+}, and Pb^{2}, Journal of Hazardous Materials 157 (2–3) (2008) 587–598.
[43] G.E. De Benedetto, R. Laviano, L. Sabbatini, P.G. Zambonin, Infrered spectroscopy in the mineralogical characterization of ancient pottery, Journal of Cultural Heritage 3 (3) (2002) 177–186.
[44] X.F. Gao, Y. Lo, C.M. Tam, C.Y. Chung, Analysis of the infrared spectrum and microstructure of hardened cement paste, Cement and Concrete Research 29 (1999) 805–812.
[45] T. Bakharev, Durability of geopolymer materials in sodium and magnesium sulfate, Cement and Concrete Research 35 (6) (2005) 1233–1246.
[46] J. Davidovits, In: IUPAC International Symposium on Macromolecules, Topic III, New Polymers of High Stability, Stockholm, 1976.
[47] K. Yip Christina, C. Lukey Grant, L. Provis John, S.J. Van Deventer Jannie, Effect of calcium silicate sources on geopolymerzation, Cement and Concrete Research 38 (2008) 554–564.
[48] V.S. Ramachandran, Application of Differential Thermal Analysis Cement Chemistry, Chemical Publishing Co., Inc., New York, 1969 55–80.
[49] 〈www.in.gov/indot/files/chapter_04.pdf〉, Chapter 4, Aggregate Specifications and Requirements.
[50] P.C. Hewlett, Lea's Chemistry of Cement and Concrete, 3rd Ed., John Wiley&Sons Inc., New York, 1998.
[51] A. Savva, P. Manita, K.K. Sideris, Influence of elevated temperature on the mechanical properties of blended cement concretes prepared with limestone and siliceous aggregates, Cement and Concrete Research 27 (2005) 239–248.